Journal of Green Chemical and Environmental Engineering

e-ISSN 3090-2568
Research Paper

Synthesis and Characterization of Composite Emulsifier from Periwinkle Shell and Gum Arabic Applied in Oil-Water Emulsification Process

Ismail O. Balogun, Ebenezer O. Dada, Kazeem K. Salam*

Department of Chemical Engineering, Faculty of Engineering and Technology, Ladoke Akintola University of Technology (LAUTECH), Ogbomoso. Oyo State. Nigeria.

** Corresponding author: kksalam@lautech.edu.ng (Kazeem K.Salam)*

Received 17 May 2025
Revised 26 May 2025
Accepted 30 June 2025

Citation: Ismail O. Balogun, Ebenezer O. Dada, and Kazeem K. Salam. (2025). "Synthesis and Characterization of Composite Emulsifier from Periwinkle Shell and Gum Arabic Applied in Oil-Water Emulsification Process". J. of Green Chemical and Environmental Engineering, Vol. 1 No.2, Page 47-65.

: 10.63288/jgcee.v1i2.6

Abstract: The Synthetic surfactants employed in the management of oil-polluted water through the emulsification process usually lead to introducing secondary pollutants with more toxic effects on the environment. However, the need to safely mitigate the environmental impact of oil pollution has led to the increasing demand for eco-friendly, bio-based materials for the treatment of oil-polluted water. The effect of Periwinkle Chitosan-Gum Arabic (PSC-GA) composite emulsifier on the stability of oil-water emulsion (10% v/v) was investigated. Chitosan was extracted from the Periwinkle shell through the sequential order of decolorization, demineralization, deproteinization, and deacetylation with 40% NaOH (DCMPA) resulting in a yield of 5.96%. The emulsifier was formed with mixtures of chitosan and gum Arabic at 0%, 1%, and 2% each dissolved in 1%, 2%, and 3% aqueous acetic acid (AA) solution in a randomized experimental design using Box Behnken Design (BBD) under Response Surface Methodology (RSM) of Design Expert (Version 13). An optimum composition of 1.10% PSC, 1.54% GA, and 1.51% AA for the emulsifier with 97.6% stability was obtained from the optimization of the emulsion stability index. This study shows that PSC-GA composite is an effective emulsifier capable of producing stable emulsion with CMC of 0.02 g/l at 0.039 N/m and Zeta potential of over -36 mV which could be applied for the emulsification process in the oil-polluted environment to prevent oil migration.

Keywords: Periwinkle Chitosan, Gum Arabic, Composite Emulsifier emulsification, oil-water, Response Surface Methodology.

1. Introduction

An emulsion is a mixture of two or more immiscible liquid phases where one phase is dispersed into another. Emulsions have been widely used in different industrial processes. The development and production of good-quality emulsions depend on the knowledge of emulsion preparation, stability mechanisms, and rheological studies. Emulsification has a very large effect on the behavior of oil spills. There are three types of emulsions which are; water-in-oil (W/O), oil-in-water (O/W), and complex emulsions such as water-in-oil-in-water (W/O/W). Emulsification is the process of emulsion formation in the presence of surfactant accompanied by homogenization. To form stable emulsions,

an emulsifier is required to reduce the droplet sizes of the emulsions and enhance the emulsion stability [1].

Emulsifiers are surface-active agents that act at the interface between the two immiscible liquids. Their main roles are to promote emulsion formation and to stabilize the emulsion. There are many types of emulsifiers with different functionalities and they are broadly grouped into synthetic and natural emulsifiers based on their sources. Synthetic emulsifiers which are usually composed of nonionic and anionic surfactants in hydrocarbon or water-hydrocarbon mixture solvents are surface-active agents designed to disperse oil in water thereby promoting the formation of oil-in-water emulsions [2]. The growing concern over their toxicity and long-term ecological effects has led to the incorporation of bio-based components in some of the latest developments [3]. While synthetic emulsifiers remain crucial in oil spill response, their adverse environmental impact has led to a shift towards bio-based alternatives. The global focus is now on green chemistry innovations and stricter regulations for ecological sustainability.

The natural emulsifiers are either animal-based or plant-based. Animal-based emulsifiers are natural surfactants derived from biological materials such as proteins, lipids, and other biomolecules found in animal byproducts. They are being explored in emulsion formation especially in oil spill cleanup due to their surface-active properties, non-toxicity, and biodegradability [4]. Examples of animal-based emulsifiers are chitosan, keratin, lecithin, fish protein hydrolysates, etc. Almost all of these animal-based emulsifiers are been consumed in food processing and pharmaceutical industries thereby limiting their availability for oil spill management. Plant-based emulsifiers are natural surfactants from different plant sources. They are developed by the extraction and modification of biopolymers, saponins, phospholipids, and polysaccharides from plant sources such as acacia trees, soybeans, quillaja bark, sugar beet, etc. These emulsifiers function by reducing interfacial tension between oil and water, stabilizing oil droplets, and enhancing microbial biodegradation. Examples of plant-based emulsifiers include gum Arabic, lecithin, saponins, xanthan gum, etc.[5].

Periwinkle shells have been used for both construction and non-construction purposes [6]. Badmus *et al*., (2007) used the periwinkle shell ash at 300°C for 2 hours and sieved with a 180 µm sieve in the removal of lead ions and copper from industrial waste waters. Periwinkle shells, like snails and other Crustaceans and Molluscs shells, contain some amounts of chitin, the precursor of chitosan [7], [8]. Chitosan is a polysaccharide containing N-acetyl-D-glucosamine residue in its C2 position, and this composed structure is responsible for the electrostatic interaction between chitosan and oil-water emulsion, hence behaves as an emulsifier [9]. One biomaterial cannot be used in all kinds of oil-water separation scenarios because different biomaterials and different oils have different characteristics. Some of the biomaterials can effectively remove oil at low pH, and some of them may effortlessly work in a different environmental condition. Chemically hydrophilic moieties can be added to a chitosan structure, and this helps to form more stable amphiphilic chitosan [10].

The emulsifying property of Chitosan as a result of its electrostatic interaction with oil-water emulsion and the availability of Periwinkle shell waste in the various community markets around the oil-producing areas is the motivating factor for this investigation.

2. Research and Methodology

2.1. Materials

The Periwinkle Shell (PS) was sourced from the popular Oyingbo market in Lagos and the simulated oil spill water was prepared in the laboratory with petroleum product (Diesel) purchased

from a local filling station in Ogbomoso, Oyo State. Hydrochloric acid (HCl), Acetic acid (CH_3COOH), and Sodium hydroxide (NaOH) used were of analytical grade and did not pass through any further pre-treatment step before their application. Distilled water was sourced from the Department of Pure and Applied Chemistry, LAUTECH, Ogbomoso, Nigeria.

2.2. Experiments

The PS was thoroughly washed with water to remove dirt and remnants of the periwinkle meat and then spread under the sun to allow the water to dry. This was followed by oven drying at 60 °C for 48 hours [11]. The dried PS was milled into powder and stored in a sealed plastic container. Chitosan was extracted from the PSP in the sequential order of Decolorization, Demineralization, Deprotenisation, and Deacetylation [12].

2.2.1. Extraction of Periwinkle Shell Chitosan

Decolorizing was carried out by measuring 500 ml of acetone into 200 g of PSP in a conical flask. The mixture was stirred for 10 minutes followed by decantation and removal of the resulting residues. The discolored PSP was obtained by washing the residue with distilled water then filtered and dried for 12 hours at 60 °C in preparation for further processing [13].

Demineralization was achieved with the addition of 4% HCl (v/v) at room temperature to the decolorized PSP with a solid-to-solvent ratio of 1:15 (w/v) for 24 hours for the elimination of calcium carbonate ($CaCO_3$) in dilute acidic medium. The residue was washed to neutral pH with distilled water, filtered, and dried at 60 °C for 20 hours (Obiefuna and Okafor, 2024).

Deprotenisation of the demineralized PSP was achieved with 10% NaOH at a solid (demineralized dried PSP) to solvent ratio of 1:15 (w/v) at 80 °C for 12 hours through constant stirring for the removal of the protein content of PSP. The residue was washed to neutral pH, filtered, and then oven-dried at 60 °C for 24 hours (Samuel et al., 2024).

Chitosan is obtained from chitin through deacetylation. This experimental step was conducted by treating the deprotenised PSP with 40% NaOH (w/v) solution for 2 hours at 110 °C with to solvent ratio of 1:15 (w/v) for the partial removal of acetyl groups from chitin structure to convert it to chitosan. The mixture was filtered and the solid materials were washed with distilled water to neutral pH. The residue was dried at 60 °C for 24 hours and stored in an airtight container at room temperature [12]

2.2.2. Preparation of PSC-GA Emulsifier

The PSC-GA emulsifier was produced using the modified methodologies [16], [17]. Acetic acid at concentrations of 1%, 2%, and 3% (v/v) was used to prepare PSC-GA solutions at room temperature. Chitosan samples at 0%, 1%, and 2% (w/v) were dissolved in the specific acetic acid with continuous stirring followed by GA (also at 0%, 1%, and 2% w/v). The stirring continued until it completely dissolved. The PSC-GA solution was used in the treatment of simulated polluted water. 4 ml of the emulsifier solution was used to form an emulsion with 100 ml of oil-polluted water (10% v/v) and the stability of the emulsion was monitored for 4 week period at 30-minute intervals for the first 24 hours.

2.2.3. Design of Experiment of Synthesis of PSC-GA Emulsifier

The experimental test matrix used for the determination of the best mixing condition of the PSC-GA blend is shown in Table 1. Box Behnken Design (BBD) under Response Surface Methodology (RSM) of Design-Expert version 13 was deployed to determine the condition that optimized the effects of the variables on the performance of the PSC-GA blend. The experimental

design matrix obtained from BDD is shown in Table 2. It has been reported that hydrolysis of Chitosan affects the solubility of Chitosan solution in distilled water with time, temperature, and blend of Chitosan and GA [18]; [19]. The optimum condition was used for the generation of regression models for the prediction of the stability of the emulsion formed with the blended PSC-GA solution. Analysis of Variance, coefficient of determination (R^2), adjusted R^2, and cross plot were used for the determination of the accuracy of the regression model developed (Agarry et al., 2024; Oke et al., 2024).

Table 1. Parameters selected for experimental design

Parameter	Unit	Low	High
PSC	%	0	2
GA	%	0	2
AA	%	1	3
Time	Min	30	90
PSC: GA	-	2	4

PSC: Periwinkle Shell Chitosan, GA: Gum Arabic, AA: Acetic Acid solution

2.2.4. Preparation of Emulsion with the PSC-GA Emulsifier

The best PSC-GA blend was determined and used as an emulsifier in the treatment of oil-polluted water. Simulated oil-polluted water was prepared by adopting the method of Aliyu *et al*. (2020) with modification by mixing 10 ml of diesel oil with 90 ml of distilled water (i.e.10% conc.). The emulsion was prepared by adding three concentrations (2%, 3%, and 4%) of the PSC-GA emulsifier to oil-polluted water and homogenized at 10,000 rpm for 2 minutes (Salam et al., 2023). The emulsion formed in each case was poured into a graduated cylinder where the stability index was monitored at 30-minute intervals until there was no further separation. The effect of pH and salinity were tested by modifying pH with HCl (0.1 M) and NaOH (0.1 M) while salinity was modified using a 4% NaCl solution [17].

Table 2. Experimental Design Matrix using Box Behnken Design (BBD)

Std	Run	A: PSC, g	B: GA, g	C: AA, %
3	1	0	2	2
16	2	1	1	2
17	3	1	1	2
5	4	0	1	1
8	5	2	1	3
9	6	1	0	1
10	7	1	2	1
11	8	1	0	3
13	9	1	1	2
2	10	2	0	2
6	11	2	1	1

4	12	2	2	2
1	13	0	0	2
15	14	1	1	2
12	15	1	2	3
14	16	1	1	2
7	17	0	1	3

2.3. Characterization of Periwinkle Shell Chitosan (PSC)

The produced chitosan, GA, and PSC-GA are characterized according to the appropriate ASTM or published references. The American Standards for Testing and Measurements (ASTM) standard of Yield of obtained PS (ASTM C 138), Degree of acetylation (ASTM F2260-18), Thermographic Analysis (TGA) (ASTM E1131), Fourier Transform Infra Radiation (FTIR) (ASTM E1252), Scanning Electron Microscopy (SEM)/Electron Dispersive X-Ray Spectroscopy (EDX) (ASTM F 1375), Surface Tension (ASTM D1331-20), Zeta Potential and Particle size analysis (ASTM E2865-12) were used in the characterization.

3. Results and Discussion

3.1. Yield and Degree of Deacetylation of PSC

The weight of dried Chitosan compared with the weight of raw periwinkle shell powder according to equation 1, a yield of 5.96% was obtained. It was stated by [11] that yield of chitosan from periwinkle shell source range from 0.44 to 71% has been recorded by different researchers. The degree of deacetylation (DD) of the chitosan sample from the FTIR analysis was obtained to be 39.72%. This conforms with DD of 40.19% recorded by [23] using a similar concentration of NaOH for the deacetylation process. A degree of deacetylation of between 30 and 95% has so far been recorded [24].

3.2. TGA Analysis of PSC and PSC-GA

Thermal stability of PSC and PSC-GA as recorded in the results of the TGA analysis in Figure 1 shows significant initial weight loss at 98 °C for PSC (Figure 1a) while 5 % initial weight loss was experienced with PSC-GA at the same temperature. There was a marginal weight loss at 200 ℃ and 160 ℃ for both PSC and PSC-GA with a weight loss of 2 and 6% respectively, this behavior represents the loss of water or moisture content [25]. The second stage (or main) degradation was observed between approximately 250 °C and 332 °C for PSC with a sharp decline starting around 260 °C, where the onset is marked while that of PSC-GA starts at 160 °C (onset temperature) and ends at 395°C which indicates a complex degradation involving multiple components. The total weight loss of 89.60% and 87.54% for PSC and PSC-GA mixture respectively from room temperature up to 600°C suggests the formation of a more thermally stable material by the interaction between chitosan and gum Arabic.

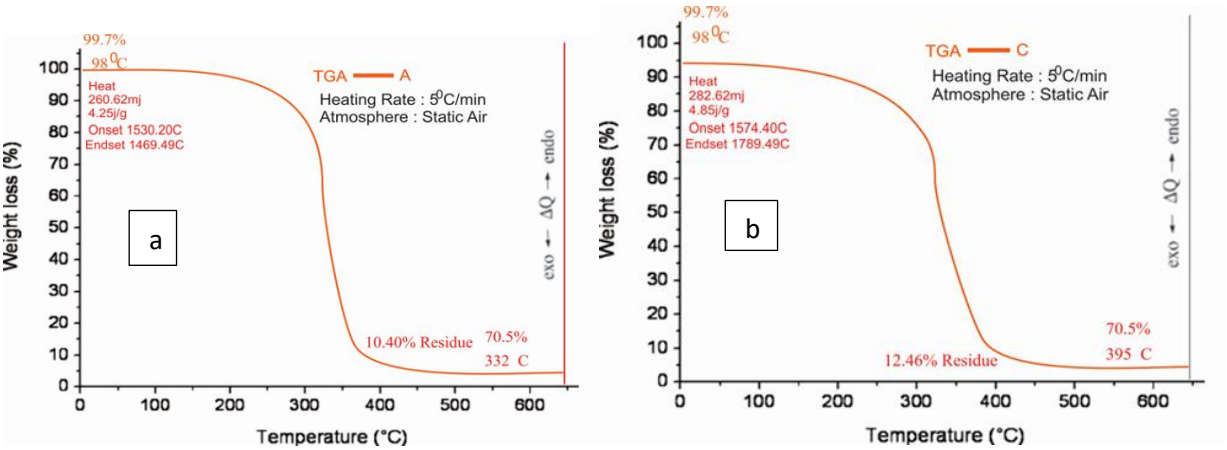

Figure 1. TGA curves of PSC (a) and PSC-GA (b)

3.3. FTIR Analysis of PSP, GA, PSC, and PSC-GA

The presence of inherent functional groups in materials and change in functional group arrangement after modification of PSP, GA, PSC, and PSC-GA were presented by the FTIR spectra recorded within the frequency range of 4000 cm^{-1} to 500 cm^{-1} using FT-IR spectrometer (Infrared spectrometer Varian 660 MidIR Dual MCT/DTGS Bundle with ATR) Shown in Figures 4a-d. The peaks and their assignments in the PSC sample matched the functional groups present in commercial chitosan with possible interactions or modifications [23]. This typical spectrum reflects chitosan's molecular structure, notably its glucosamine backbone interlaced with acetylated and deacetylated units. The shifting of some peaks and increase in the intensity of some bands as noticed from PSP to PSC and PSC-GA is indicative of modifications that lead to the formation of a spectrum which does not as prominently feature in the lower wave number peaks (1150-1030 cm^{-1}) seen in pure chitosan, or they have shifted as seen in PSC-GA due to the blend, which might affect the observation of pure saccharide signals.

The peak at 3413.35 cm^{-1} is typically attributed to the O-H and N-H stretching vibrations of hydroxyl and amine groups respectively (Figure 4.3a). The hydrogen bonding interactions often cause the broad nature of this peak. The peak at 2917.87 cm^{-1} was assigned to the C-H stretching vibrations of methyl and methylene groups, indicating the presence of aliphatic hydrocarbons in the chitosan structure. The Amide peaks around 1650.03 cm^{-1} and 1562.52 cm^{-1} are related to the amide I and amide II bands of proteinaceous residues or the N-H bending vibration coupled with C=N stretching (from residual acetylation of chitosan) suggesting the presence of chitosan but seen at slightly shifted positions in the PSC-GA (Figure 4.3b), possibly due to interactions with gum Arabic.

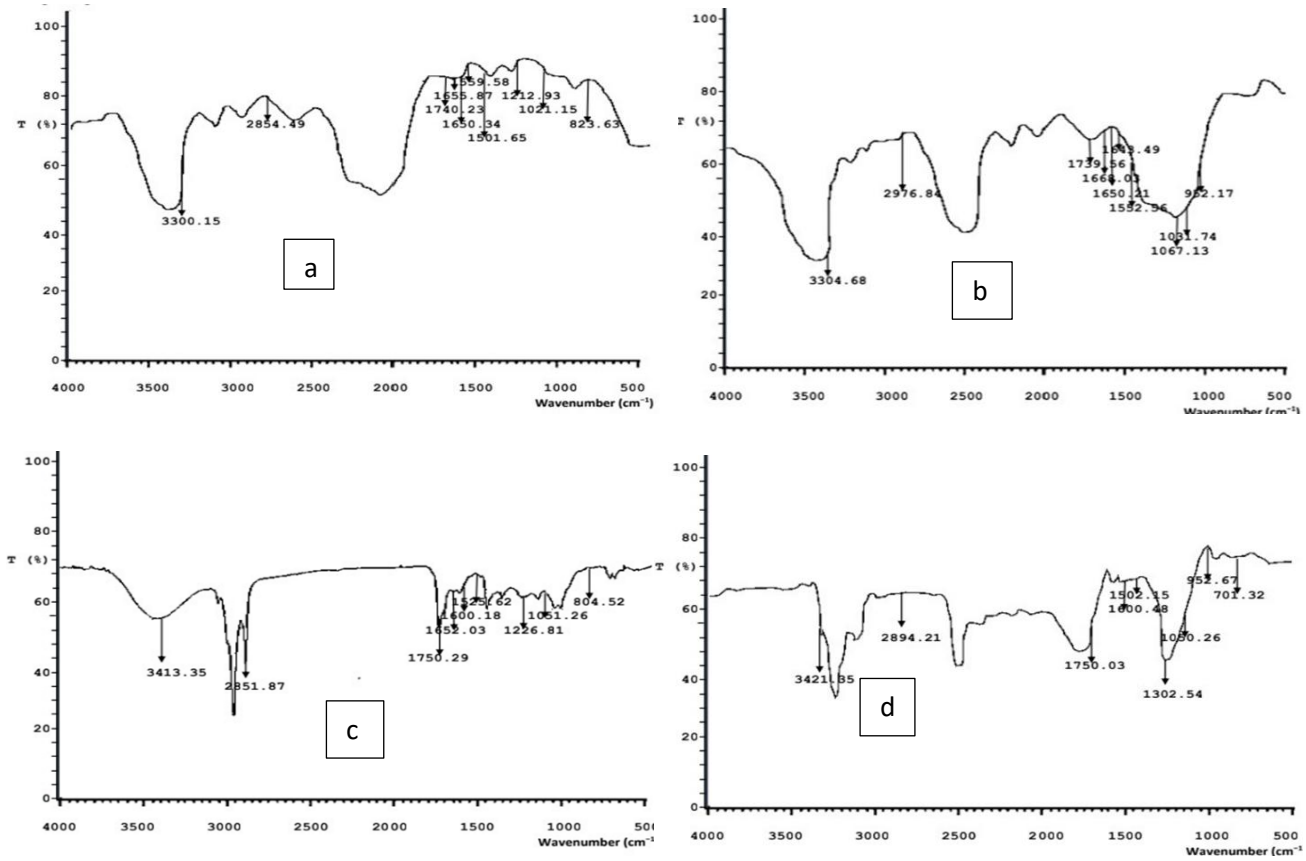

Figure 2. FTIR spectrum of GA (a), PSP (b), PSC (c) and PSC-GA (d)

Table 3. Summary of different functional groups presented in PSP, GA, PSC, and PSC-GA

Vibration	Wave Number(cm-^{1})			
	PSP	GA	PSC	PSC-GA
O-H Stretch	3304.68	3300.15	3413.35	3421.35
C-H Stretch	2976.84	2854.49	2851.87	2894.21
C-N Stretch	1668.13	1655.87	1600.18	1600.48
C-O Stretch	1650.21	1650.34	--	---
O-H Bend	1643.49	--	--	---
N-H Bend	1552.56	1559.58	1525.62	1502.67

3.4. SEM and EDX Analysis

The SEM image of PSC (Figure 3a) indicated particles that are heterogeneous in size, shape, and texture. The shape ranges from relatively flat and irregular to more round with a lump of particles on its surface and crevices layers. This variability is common in polymer structures, influenced by the synthesis and drying processes. The texture and porosity visible in the SEM image suggest that it might have good reactive and absorptive properties due to the increased surface area [24].A heterogeneous mixture of particles that appeared to have a relatively irregular and non-spherical shape with rough texture and variable sizes was observed in the PSC-GA image (Figure 3b). Some particles seemed to aggregate, indicating possible interaction between PSC-GA

molecules, which might lead to different bonding and structural properties compared to pure substances. The granular and aggregated appearance suggested that the addition of GA modified the regular PSC structure, leading to the formation of these new particle morphologies.

In the EDX spectrum of PSC (Figure 4a), prominent peaks are evident for elements like Carbon, Oxygen, Sodium, Iron, Copper, Manganese, Calcium, Zinc, Magnesium, Silicon, and Phosphorus. From the image, it appeared that the most pronounced peaks are for Carbon and Oxygen, which is typical for chitosan since it is primarily composed of these elements in its structure. The presence of elements like Iron, Copper, Manganese, Zinc, and Silicon suggest impurities within the sample, possibly incorporated during the preparation process or as part of the materials used in synthesizing the PSC.

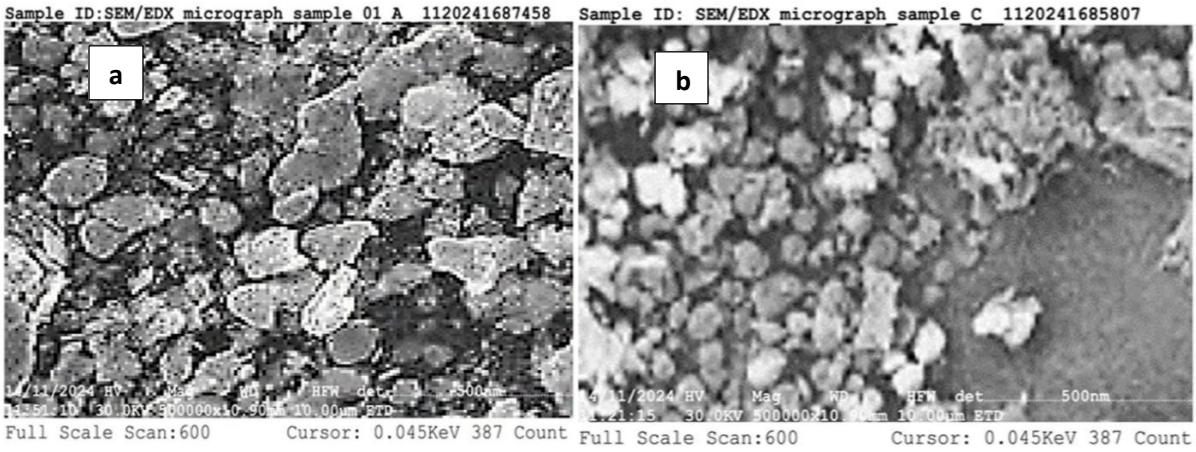

Figure 3. SEM image of PSC (a) and PSC-GA (b)

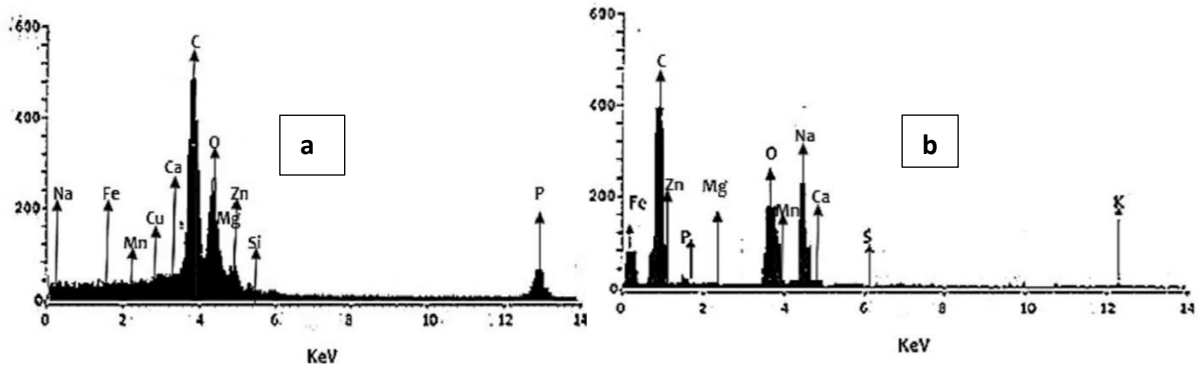

Figure 4. EDX chart of (a) PSC and (b) PSC-GA

Figure 4b showed significant peaks for carbon and oxygen, which are the primary constituents of both PSC and GA in different proportions. These natural polymers are composed predominantly of carbon, hydrogen, and oxygen, derived from their polysaccharide structure. The chart also showed peaks for sodium (Na), magnesium (Mg), phosphorus (P), sulfur (S), calcium (Ca), and potassium (K). The presence of these elements might be due to the intrinsic properties of GA, which contains various salts, or from the processing environment.

Table 4. Quality parameters of PSC and PSC-GA from SEM/EDX

Parameter	PSC	PSC-GA
Shape	Relatively flat and irregular to more round	Irregular and non-spherical
Particle size (μm)	1.11	1.63
Height (mm)	1.37	1.27
Bulk density (g/cm^3)	1.07	1.59

Table 5. Elemental Composition of PSC and PSC-GA from EDX

Element	Composition (%)		
	PSC	PSC-GA	Commercial Chitosan(CS)*
Carbon (C)	51.33	57.85	48.2
Oxygen (O)	26.41	20.43	28.8
Phosphorous (P)	8.15	0.82	---
Calcium (Ca)	3.27	3.16	3.2
Potassium (K)	---	1.05	---
Sodium (Na)	2.35	7.15	5.9
Zinc (Zn)	4.03	0.02	---
Iron (Fe)	0.61	9.28	---
Magnesium (Mg)	2.23	0.15	1.2
Copper (Cu)	1.19	–	---
Manganese (Mn)	0.41	0.08	---
Chlorine (Cl)	---	---	0.6
Aluminium (Al)	---	---	0.4

*Al Balushi *et al*., 2021

3.5. BET Analysis Result

The BET (Brunauer-Emmett-Teller) surface area plot for both PSC and PSC-GA (Figure 6a and b) showed a mostly linear increase from P/P0 = 0 to about 0.9. The slope in this range is constant, suggesting a uniform adsorption process. The direct proportionality seen up to P/P0 = 0.9 suggested the adsorption is mostly limited to the formation of a monolayer on the surface of the materials. The linear correlation of the PSC-GA Mixture plot, suggests that the material adheres well to the BET model within the relative pressure range shown (approximately 0.05 to 0.9). This linearity is crucial because the BET theory is valid typically in a relative pressure range of about 0.05 to 0.35 for most materials.

The Barrett-Joyner-Halenda (BJH) adsorption cumulative pore volume analysis for the chitosan sample (Figure 5a) showed a trend in which as the pore width increases, the cumulative volume of pores decreases sharply initially and then levels off more gradually. This suggests a higher volume of smaller pores within the PSC sample. There is a significant decrease in cumulative pore volume as pore width increases from around 10 Å to approximately 200 Å for both PSC and PSC-GA, indicating a large distribution of small pores in both. The significant drop in pore volume observed as the pore width moves from about 10 Å to around 100 Å followed by a decline at a less

steep rate suggested that the majority of pores in both materials are microporous (less than 20 Å) and mesoporous (20 Å to 500 Å) with few amount of lager pores.

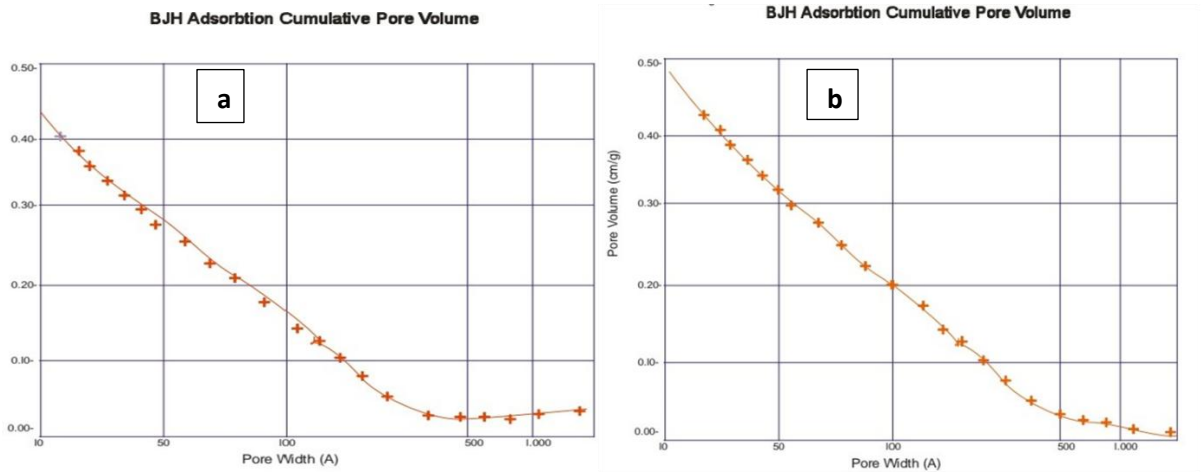

Figure 5. BET-BJH adsorbtion cumulative pore volume for PSC (a) and PSC-GA (b).

Table 6. Summary of BET parameters for PSC and PSC-GA

Parameters	PSC	PSC-GA
BET Surface area (m^2/g)	260.35	275.52
Langmuir surface area (m^2/g)	150.22	152.52
Total Pure volume (cm^3/g)	0.55	0.58
t-plot Micropore area (cm^2/g)	20.20	22.40
Average Pore width (nm)	2.83	2.80
BJH Adsorption Cumulative surface area(m^2/g)	50.20	50.22

The summary of the BET analysis of PSC and PSC-GA as tabulated in Table 6 shows a slightly increased BET surface area when PSC was modified to PSC-GA composite from 260.35 to 275.52 m^2/g. The values of the other considered BET parameters are approximately the same after the synthesis of the PSC-GA emulsifier.

3.6. Modeling of Emulsification of Oil-Polluted Water with PSC-GA.

3.6.1. Effect of Composition on Stability of PSC-GA Emulsifier

Based on the experimental design of Table 2, seventeen (17) experimental runs were generated. Four out of these seventeen runs (i.e. runs 6,8,10 and 13) were unable to facilitate the formation of emulsion and separated immediately after homogenization. These four experimental runs do not have GA in their formulations while others with GA produced stable emulsions with stability between 84 – 89 % as shown in Table 7. This demonstrated that the presence of GA in the emulsifier prepared from the mixture of PSC and GA aided in the formation of a stable emulsion. The maximum stability observed was achieved at run 15 (PSC, GA, and AA of 1 g, 2 g, and 3%).

3.6.2. Analysis of Variance (ANOVA) and Model Evaluation

The data presented was used for the development of the regression model shown in Equation 4. The equation has 3 main terms, two-interactive model terms and two quadratic model terms. The ANOVA of the developed model for the stability of emulsion prepared from the synthesized PSC-GA composite was tabulated in Table 4.6. The Model F-value of 3270.24 implies the model is significant. There is only a 0.01% chance that an F-value this large could occur due to noise. P-values less than 0.0500 indicate model terms are significant. In this case B, AC, A^2, B^2 are significant model terms. Values greater than 0.1000 indicate the model terms are not significant. If there are many insignificant model terms (not counting those required to support hierarchy), model reduction may improve the model. The Lack of Fit F-value of 1.46 implies the Lack of Fit is not significant relative to the pure error. There is a 36.80% chance that a Lack of Fit F-value this large could occur due to noise.

Stability = +3.29079-0.263158 PSC+127.76184 GA-1.82500 AA + 1.30000 PSC*AA+0.750000 GA*AA -1.31842 PSC^2-42.86842 GA^2 (4)

Table 7. Experimental design matrix of Emulsion Stability Index (ESI)

Std	Run	A: PSC, g	B: GA, g	C: AA, %	Stability, %
3	1	0	2	2	87.2
16	2	1	1	2	86
17	3	1	1	2	88
5	4	0	1	1	87.2
8	5	2	1	3	86
9	6	1	0	1	0
10	7	1	2	1	86
11	8	1	0	3	0
13	9	1	1	2	88
2	10	2	0	2	0
6	11	2	1	1	84
4	12	2	2	2	86
1	13	0	0	2	0
15	14	1	1	2	87
12	15	1	2	3	89
14	16	1	1	2	88
7	17	0	1	3	84

The Predicted R^2 of 0.9979 is in reasonable agreement with the Adjusted R^2 of 0.9993; i.e. the difference is less than 0.2 (Table 4.7). Adeq Precision measures the signal-to-noise ratio. A ratio greater than 4 is desirable. The ratio of 130.418 indicates an adequate signal. The obtained results for the parameters used to test the accuracy of the model show that the developed model for the prediction of the stability of oil-water emulsion in the presence of PSC-GA was within the specified limits for prediction purposes [27], [28].

Table 8. Model Statistics for Emulsion Stability Response

Source	Sum of Squares	df	Mean Square	F-value	p-value	
Model	22982.71	7	3283.24	3270.24	< 0.0001	significant
A-PSC	0.7200	1	0.7200	0.7171	0.4190	
B-GA	15155.41	1	15155.41	15095.38	< 0.0001	
C-AA	0.4050	1	0.4050	0.4034	0.5411	
AC	6.76	1	6.76	6.73	0.0290	
BC	2.25	1	2.25	2.24	0.1686	
A^2	7.34	1	7.34	7.31	0.0242	
B^2	7759.18	1	7759.18	7728.45	< 0.0001	
Residual	9.04	9	1.00			
Lack of Fit	5.84	5	1.17	1.46	0.3680	not significant
Pure Error	3.20	4	0.8000			
Cor Total	22991.74	16				

Table 9. Fit summary of emulsion stability

Parameter	Value
Std. dev.	1.00
Mean	66.26
C.V. %	1.51
R^2	0.9996
Adjusted R^2	0.9993
Predicted R^2	0.9979
Adeq. Precision	130.4176

3.6.3. Perturbation Plots of Emulsion Stability

A perturbation plot was used for the determination of the effect of each of the components used for the developed regression models considering only one component at a time while the other components' values are fixed at their respective midpoint values (Figure 6).The increase in PSC (component A) from 0 to 2 g keeping B and C at their midpoint values led to a marginal increase in emulsion stability from 85% at 0 to 88% at 1 g.Further increase of PSC beyond 1 g led to a decrease in stability to 85% at 2 g. An increase in GA (component B) led to an increase in emulsion stability from 85% at 0 to 95% at 1.5 g followed by a slight decrease in stability at a further increase of GA to 87% at 2 g of GA. Change in AA composition (component C) from 1% to 3% has no significant effect as the stability remains at 85% for the increase from 1 to 3% acetic acid composition.

3.6.4. 3D Surface Plot of Interaction between parameters

The surface plot describes the relationship between the simultaneous increase in the values of two variables (two factors) on the output or response, while the remaining factors are kept constant at their midpoint values. The interaction between GA (B) and AA (C) (Figure 7a) at a low value of C shows a stability of 1.18% at 0 value of B and 97.32% at 1.47g of B which decline to 86.73% at further increase of B to 2g. At a high value of C, the stability moved from 0.13% at 0 value of B to 99.6% at B of 1.43g. An increase of B to 2g gives a stability of 88.68%. While the AC interaction (Figure 7b) does not show a significant variation in the stability at either a low or high value of C no matter the increase in A. At a low value of C, the stability was 87.11% for 0 value of A and 83.91% at 2g of A. At high C, the stability was 84.96% and 86.96% for 0 and 2g of A respectively.

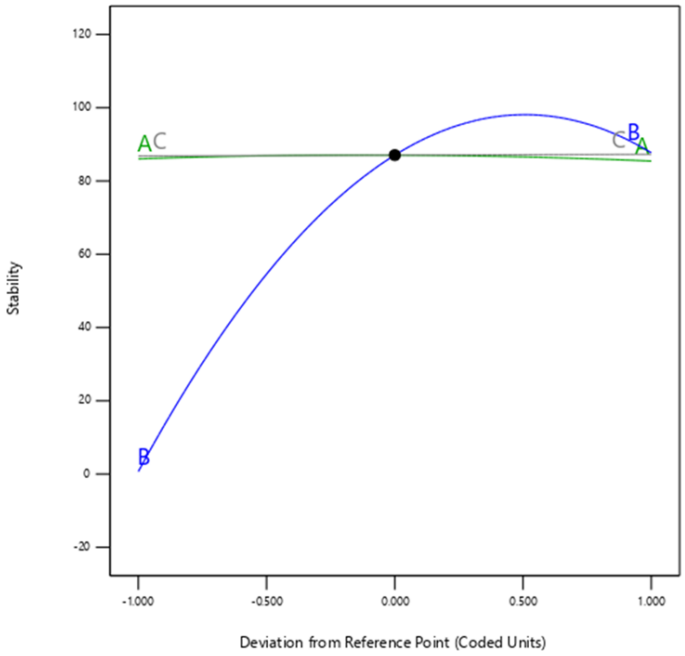

Figure 6. Perturbation plots of the effect of each of the components on emulsion stability

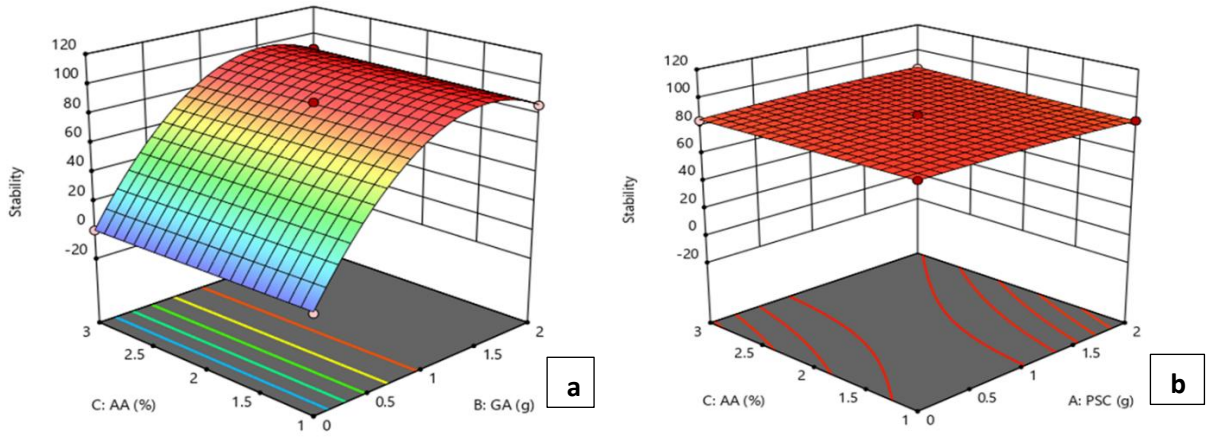

Figure 7. 3D Surface Plot showing the Effects of each component on Emulsion Stability (a) GA-AA (b) PSC-AA

3.6.5. Optimization Study of the Stability of Produced Emulsion

The prediction of the stability of emulsion produced from oil and water with synthesized PSC-GA as an emulsifier was performed via a numerical optimization tool in the Design Expert v13 using a published methodology(Salam, et al., 2023). The numerical optimization method was used to determine the best PSC, GA, and AA within the experimental range specified in Table 1. The ramp of the optimization of the values of the input factors and stability is presented in Figure 8. The values of PSC, GA, and AA that produced a stability of 97.6% are 1.10 g, 1.54 g, and 1.51%. The predicted values in the ramp of optimization were validated in the laboratory by conducting a passing experiment. The result produced an emulsion with a stability of 96.51%. The deviation of the experimental value and the predicted values was 1.12%.

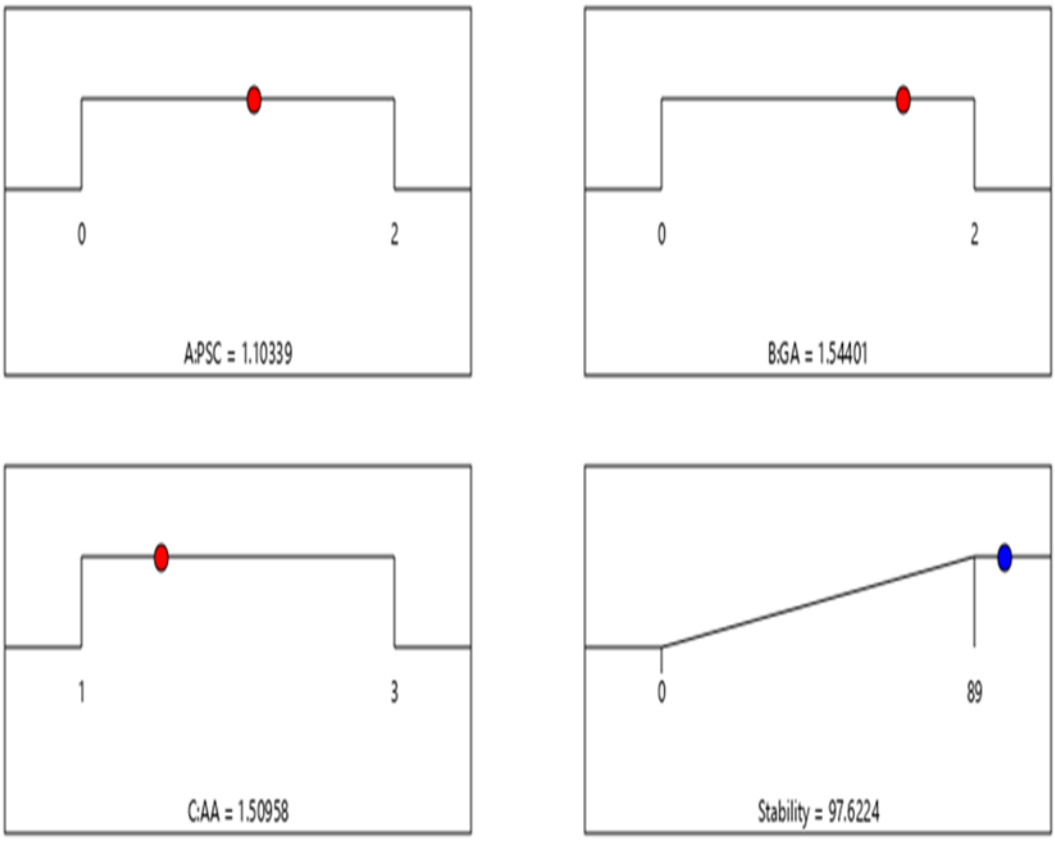

Figure 8. Optimization of the developed emulsion stability model.

3.7. Characterization of the Produced Emulsion

3.7.1. Surface Tension and CMC of the Emulsifier

The surface tension of the emulsifier, (PSC-GA) was tested and compared with that of PSC by dissolving 1g of each in 100 ml of kerosene separately, with a serial dilution of 0.05, 0.010, 0.020, and 0.025g/l of each sample solution. Initially, as the concentration of the sample increases from 0.005 g/L, the surface tension decreases sharply. At a certain concentration of around 0.015 g/L (for PSC) and 0.02 g/L (for PSC-GA), the surface tension reaches a minimum and stabilizes (Figure 9a and b). This point is referred to as the Critical Micelle Concentration (CMC) above which micelles begin to form in the solution. Beyond this concentration, the surfactant molecules self-assemble into micelles and an increase in concentration beyond the CMC does not significantly alter the surface

tension. The surface tension of the PSC was 0.44 at CMC and reduced to 0.40 for PSC-GA at 0.02 g/L

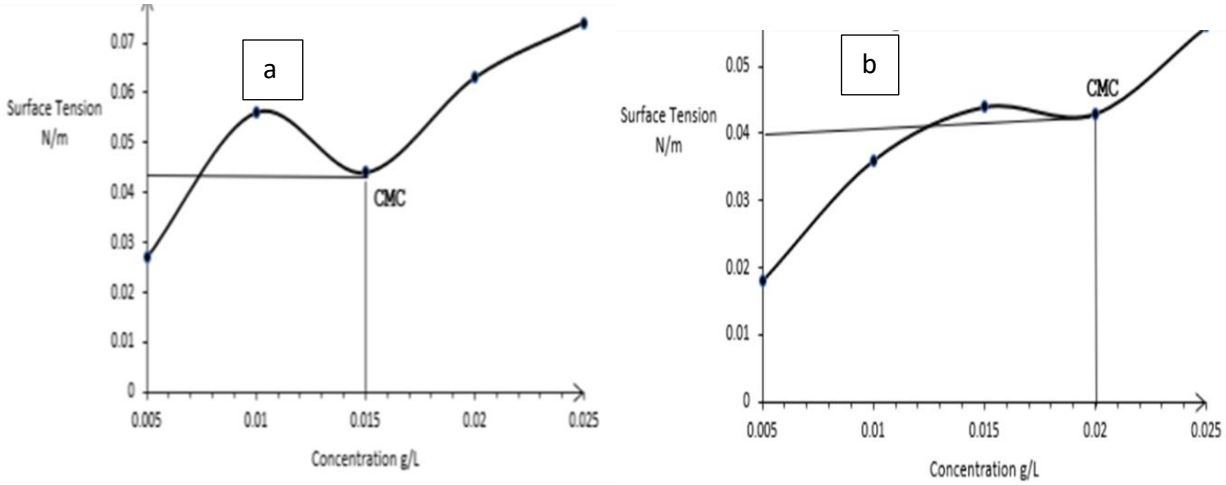

Figure 9. Surface tension plot for PSC (a) and PSC-GA (b) at different concentrations

3.7.2. Particle Size Distribution and Zeta Potential of the Emulsion

Particle size distributions of PSC-GA emulsion were evaluated as functions of volume, number, and intensity (Figure 10). The results showed a uniform distribution pattern with an average size of 43.34 d.nm. A peak at -36 mV, was observed from the Zeta potential plot of the emulsion as shown in Figure 11, suggesting that most particles in the sample have a zeta potential around this value. Zeta potential is a key indicator of the stability of colloidal dispersions and emulsions. It measures the magnitude of the electrostatic or charge repulsion/attraction between particles. The peak at -36 mV indicates that the particles have very strong electrostatic repulsion [30]. This is indicative of the high stability of the emulsions. This is desirable because the emulsion is intentionally desired to be stable to prevent further migration of oil and also encourage biodegradation.

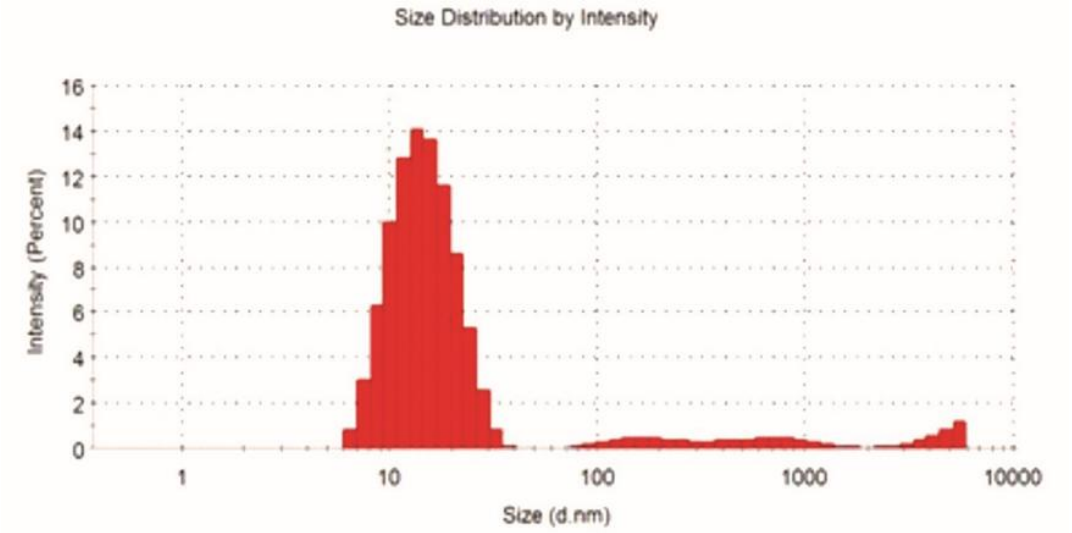

Figure 10. Size distribution as a function of particle intensity

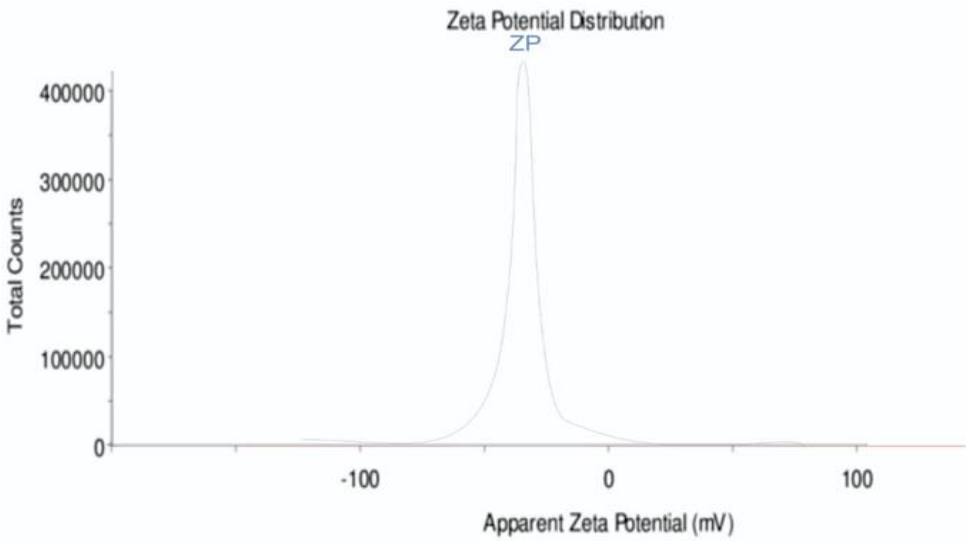

Figure 11. Zeta potential distribution of PSC-GA emulsion with oil-polluted water

4. Conclusion

Chitosan was successfully synthesized from PS waste with a yield of 5.96% and a degree of deacetylation of 39.72%. Modification of PSC to PSC-GA emulsifier was achieved with 96.51% stability of the emulsion formed. The TGA analysis showed decreased onset degradation of PSC relative to PSC-GA by 20%, this led to an increase in final degradation temperature by 18.98% and increased residue content by 19.23%. The functional groups present in the PSC are also noticed on the PSC-GA composite though at varied wavelengths. The C-O content in the PSC was within the specified range in the literature (greater than 1.5) and also increased from 1.94 to 2.8 after modification of PSC to PSC-GA. The model developed for the stability of the produced emulsion was desirable with R2, Adjusted and Predicted R2 of 0.9996, 0.9993, and 0.9979. The validation of the 96.51% stability of the produced emulsion was achieved at PSC of 1.10 g, GA of 1.54 g, and AA of 1.51% with a deviation of 1.11%. The high stability of emulsion obtained from this optimum composition is necessary for the prevention of spilled oil migration and the promotion of biodegradation of pollutant oil. The stability of the emulsion formed was confirmed by the zeta potential value of -36 mV and a particle size distribution with an average size of 43.34 nm.

Author contributions: Conceptualization, KKS. and EOD; data curation, IOB; formal analysis, IOB; investigation, IOB; methodology, KKS & EOD; project administration, KKS & EOD, resources, KKS & EOD; software, KKS & EOD; supervision, KKS & EOD; validation, IOB; visualization, IOB; writing—original draft preparation, IOB; writing—review and editing, KKS & EOD. All authors have read and agreed to the published version of the manuscript.

Conflict of Interest: The authors declare that there are no conflicts of interest.

5. References

[1] S. Akbari and A. H. Nour, “Emulsion types , stability mechanisms and rheology : A review Emulsion types , stability mechanisms and rheology : A review,” no. October, 2020, doi: https://doi.org/10.53894/ijirss.v1i1.4.

[2] J. Chen and P. Xia, “Health effects of synthetic additives and the substitution potential of plant-based additives,” *Food Research International*, vol. 197, p. 115177, 2024, doi: https://doi.org/10.1016/j.foodres.2024.115177.

[3] I. Dammak, P. Sobral, A. Aquino, M. Neves, and C. Conte Junior, “Nanoemulsions: Using emulsifiers from natural sources replacing synthetic ones—A review,” *Compr Rev Food Sci Food Saf*, vol. 19, Aug. 2020, doi: https://doi.org/10.1111/1541-4337.12606.

[4] Z. Chen, C. An, Y. Wang, B. Zhang, X. Tian, and K. Lee, “A green initiative for oiled sand cleanup using chitosan/rhamnolipid complex dispersion with pH-stimulus response,” *Chemosphere*, vol. 288, p. 132628, 2022, doi: https://doi.org/10.1016/j.chemosphere.2021.132628.

[5] A. N. Adharsh and M. Sontakke, “Plant-based emulsifiers : Sources , extraction , properties and applications,” vol. 12, no. 5, pp. 8–16, 2023.

[6] I. E. Ekop, K. J. Simonyan, and U. N. Onwuka, “Comparative analysis of mechanical properties of two varieties of periwinkle relevant to the design of cracking unit of the shelling machine,” vol. 24, no. 2, pp. 122–136, 2022.

[7] H. Hemmami, I. Ben Amor, A. Ben Amor, and S. Zeghoud, “Chitosan , Its Derivatives , Sources , Preparation Methods , and Applications : A Review,” vol. 11, no. 1, pp. 341–364, 2024.

[8] A. Pellis, G. M. Guebitz, and G. S. Nyanhongo, “Chitosan : Sources , Processing and Modification Techniques,” pp. 5–25, 2022.

[9] T. Huq, A. Khan, D. Brown, N. Dhayagude, Z. He, and Y. Ni, “Sources, production and commercial applications of fungal chitosan: A review,” *Journal of Bioresources and Bioproducts*, vol. 7, no. 2, pp. 85–98, 2022, doi: https://doi.org/10.1016/j.jobab.2022.01.002.

[10] A. Chander *et al.*, “Subject index,” *Miner Eng*, vol. 10, no. 2, 2015.

[11] C. C. Odili, O. P. Gbenebor, H. A. Haffner, and S. O. Adeosun, “A Morphological Characterization of High Yield Chitin from Periwinkle Shells,” vol. 5, no. 4, pp. 61–65, 2021.

[12] A. A. Adekanmi, U. T. Adekanmi, and A. S. Adekanmi, “Production and characterisation of chitosan from chitin of snail shells by sequential modification process,” vol. 22, no. February, pp. 39–53, 2023, doi: https://doi.org/10.5897/AJB2020.17135.

[13] A. A. Adekanmi, U. T. Adekanmi, and A. S. Adekanmi, “Production and characterisation of chitosan from chitin of snail shells by sequential modification process,” vol. 22, no. February, pp. 39–53, 2023, doi: https://doi.org/10.5897/AJB2020.17135.

[14] J. N. Obiefuna and V. N. Okafor, “Comparative Studies of the Physicochemical Properties of Chitosan from Commercial and Periwinkle Shell (CPS),” vol. 1, pp. 186–191, 2024.

[15] N. Y. Samuel, A.E.; Kamber, S.Y.; Samaila, D.S.; Ilesanmi, “Preparation and Characterization of Periwinkle Shell Based Chitosan-Kenaf fibre Copolymer and its Derivatives for Selective Binding of Cu (II) and Zn (II) ions from Electroplating Effluent,” *J. Appl. Sci. Environ. Manage.*, vol. 28, no. 3, pp. 853–863, 2024.

[16] N. L. Lukman Hekiem *et al.*, “Effect of chitosan dissolved in different acetic acid concentration towards VOC sensing performance of quartz crystal microbalance overlay with chitosan,” *Mater Lett*, vol. 291, p. 129524, 2021, doi: https://doi.org/10.1016/j.matlet.2021.129524.

[17] A. A. Adewunmi, A. Mahboob, M. S. Kamal, and A. Sultan, “Pickering Emulsions Stabilized by Chitosan/Natural Acacia Gum Biopolymers: Effects of pH and Salt Concentrations,” *Polymers (Basel)*, vol. 14, no. 23, pp. 1–13, 2022, doi: https://doi.org/10.3390/polym14235270.

[18] J. Santoso, K. C. Adiputra, L. C. Soerdirga, and K. Tarman, “Effect of acetic acid hydrolysis on the characteristics of water soluble chitosan,” *IOP Conf Ser Earth Environ Sci*, vol. 414, no. 1, 2020, doi: https://doi.org/10.1088/1755-1315/414/1/012021.

[19] A. Sharkawy, M. F. Barreiro, and A. E. Rodrigues, “Preparation of chitosan/gum Arabic nanoparticles and their use as novel stabilizers in oil/water Pickering emulsions,” *Carbohydr Polym*, vol. 224, no. August, p. 115190, 2019, doi: https://doi.org/10.1016/j.carbpol.2019.115190.

[20] S. Enahoro, A. Kazeem, K. Salam, A. Olanrewaju, A. Micheal, and A. Oyelakin, “Adsorptive desulfurization of diesel with modified pig dung : experimental design with optimization , kinetics , isotherms and thermodynamics studies,” *Discover Applied Sciences*, 2024, doi: https://doi.org/10.1007/s42452-024-05859-5.

[21] E. Olusola Oke *et al.*, “Zeolite-Y-catalyst production from locally sourced Meta-kaolin: Computer-Aided scale-up process design and economic analysis with Monte-Carlo-Simulation,” *Cleaner Materials*, vol. 11, no. October 2023, 2024, doi: https://doi.org/10.1016/j.clema.2024.100233.

[22] K. K. Salam *et al.*, “Lignin extraction from sawdust : optimization of experimental studies, computer - aided simulation and techno - economic analysis of scale - up process design with uncertainty quantification,” *Systems Microbiology and Biomanufacturing*, 2023, doi: https://doi.org/10.1007/s43393-023-00197-w.

[23] I. Hermiyati and S. Juhana, “Synthesis of Chitosan from the Scales of Starry Trigger Fish (Abalistes stelaris),” pp. 3–9, 2019.

[24] Oyedeko et al, “Preparation And Characterization Of Synthetic Chitosan Using Bio-Waste (SNAIL SHELL),” vol. 4, no. September, pp. 38–46, 2019.

[25] S. Kumar and J. Koh, “Physiochemical , Optical and Biological Activity of Chitosan-Chromone Derivative for Biomedical Applications,” pp. 6102–6116, 2012, doi: https://doi.org/10.3390/ijms13056102.

[26] I. H. and I. Juhana, Swatika, “Synthesis of Chitosan from the Scales of Starry Trigger Fish (Abalistes Synthesis of Chitosan from the Scales of Starry Trigger Fish (Abalistes stelaris),” no. January, 2019, doi: https://doi.org/10.13005/ojc/350147.

[27] K. K. Salam, E. O. Oke, J. C. Ude, and U. Yahya, “Zeolite-Y-based Catalyst Synthesis from Nigerian Elefun Metakaolin: Computer-aided Batch Simulation, Response Surface and Neuro-Fuzzy Modelling Performance Evaluation with Optimization,” *Chemical Papers*, vol. 76, pp. 1213–1224, 2022.

[28] E. Olusola Oke *et al.*, “Zeolite-Y-catalyst production from locally sourced Meta-kaolin: Computer-Aided scale-up process design and economic analysis with Monte-Carlo-Simulation,” *Cleaner Materials*, vol. 11, no. October 2023, 2024, doi: https://doi.org/10.1016/j.clema.2024.100233.

[29] K. K. Salam *et al.*, “Multi-objectives regression , optimization and risk assessment of profitability indicators of the simulation of mini Liquefied Petroleum Gas (LPG) dispensing unit,” *Algerian Journal of Engineering and Technology*, vol. 08, pp. 288–301, 2023.

[30] A. Linda *et al.*, “Nanotechnology based drug delivery systems for the treatment of anterior segment eye diseases,” *Journal of Controlled Release*, vol. 354, no. January, pp. 465–488, 2023, doi: https://doi.org/10.1016/j.jconrel.2023.01.018.